Available online at www.sciencedirect.com

ScienceDirect

MATTER AND RADIATION AT EXTREMES

Matter and Radiation at Extremes 2 (2017) 129−138

www.journals.elsevier.com/matter-and-radiation-at-extremes

Research Article

Investigation of Al plasmas from thin foils irradiated by high-intensity extreme ultraviolet

E.V. Grabovski [a,*], P.V. Sasorov [b], A.P. Shevelko [c], V.V. Aleksandrov [a], S.N. Andreev [c], M.M. Basko [b], A.V. Branitski [a], A.N. Gritsuk [a], G.S. Volkov [a], Ya.N. Laukhin [a], K.N. Mitrofanov [a], G.M. Oleinik [a], A.A. Samokhin [a], V.P. Smirnov [a], I.Yu. Tolstikhina [c], I.N. Frolov [a], O.F. Yakushev [c]

[a] *State Research Center of the Russian Federation Troitsk Institute for Innovation and Fusion Research, 108840, Troitsk, Moscow, Russia*
[b] *Keldysh Institute of Applied Mathematics of the Russian Academy of Sciences, Miusskaya pl. 4, 125047, Moscow, Russia*
[c] *P.N. Lebedev Physical Institute of the Russian Academy of Sciences, Leninsky pr. 53, Moscow, 119991, Russia*

Received 30 July 2016; revised 10 November 2016; accepted 21 November 2016
Available online 1 February 2017

Abstract

Dynamics and spectral transmission of Al plasma produced by extreme ultraviolet (EUV) irradiation of 0.75-μm thick Al foil is investigated. The EUV radiation with the peak power density in the range of 0.19−0.54 TW/cm^2 is provided by Z-pinch formed by W multiwire array implosion in the Angara-5-1 facility. Geometry of the experiment ensures that there are no plasma fluxes from the pinch toward the Al foil and plasma. The same EUV source is used as a back illuminator for obtaining the absorption spectrum of Al plasma in the wavelength range of 5−24 nm. It comprises absorption lines of ions Al^{4+}, Al^{5+}, Al^{6+}, Al^{7+}. Analysis of relative intensities of the lines shows that those ions are formed in dense Al plasma with a temperature of ~20 eV. Dynamics of Al plasma has been investigated with transverse laser probing. We have also performed radiation-gas-dynamics simulations of plasma dynamics affected by external radiation, which includes self-consistent radiation transport in a plasma shell. The simulations show good agreement with an experimental absorption spectrum and with experimental data concerning plasma dynamics, as well as with the analysis of line absorption spectrum. This confirms the correctness of the physical model underlying these simulations.

PACS codes: 52.59.Qy; 52.25.Os; 52.65.-y

Keywords: Z-pinch; Dense plasma transparency

1. Introduction

Emission and absorption effects of thermal radiation in high-temperature dense plasmas are a subject of numerous experimental and theoretical studies. Experiments on heating thin foils and plastic films were carried out by using high-power lasers [1−4] and powerful Z-pinches [5,6]. Most of the experiments were based on the analysis of absorption K-spectra in foils of light elements. However, in many applications, it is necessary to know the properties of radiation-plasma interaction for plasmas having a temperature in the range of 10−100 eV, involving radiation in the spectral range of 50−400 eV (with wavelengths of 3−25 nm). The spectral range corresponds to the ranges of extreme ultraviolet (EUV) and soft X-ray radiation. Such investigations have been performed in Refs. [5] and [6] with the use of Z-pinch techniques and the most powerful facilities in the world: Saturn [5] and Z-machine [6].

* Corresponding author.
E-mail address: angara@triniti.ru (E.V. Grabovski).
Peer review under responsibility of Science and Technology Information Center, China Academy of Engineering Physics.

http://dx.doi.org/10.1016/j.mre.2016.11.007

In Ref. [5], iron foils irradiated by photons emitted by two coaxial Au-coated hohlraums have been studied. Z-pinch was formed at the axis of the primary (inner) hohlraum. This axial source filled the primary hohlraum by its radiation (500 kJ, 20 ns). The secondary (outer) hohlraum was filled by radiation passing through holes of inner hohlraum surface. The temperatures of blackbody radiation obtained in the inner and outer hohlraums were, respectively, 70 and 20 eV. A sandwiched sample was located inside the secondary hohlraum providing uniform heating and controlled temperature of the sample. Radiation from the inner hohlraum was used for backlighting as well. The sample made of $FeO_{0.41}$ and having an area density of 6.9 mg/cm^2 was placed between two layers of plastic. The sample was positioned so that the backlighting radiation passed through the iron only, not through the plastic. The dimensions of the iron sample along the ray of backlighting and in the perpendicular directions were 2–10 mm and 1 mm, respectively, at the moment of measurements. The density of iron plasma was 0.1 mg/cm^3 with a temperature of 20 eV. The absorption spectrum was measured in a photon energy range of 65–90 eV ($\lambda = 14$–19 nm).

Powerful radiation of Z-pinches in Z-machine was used in Ref. [6] for thin foil heating. The foil, made of Fe/Mg and tampered by plastic films, was installed on the axis of the emitting Z-pinch (1.5 MJ, ~9 ns). The pinch was generated by implosion of a W multiwire array with a carbon-hold foam cylinder inside. The radiation flux emitted from the end face of the foam cylinder passed through the sample of Fe/Mg-foil tampered by plastic films. The first smoother part of the radiation pulse, which was close to a 180-eV temperature, heated the sample, whereas the second shorter and harder part of the radiation pulse was used for back illumination. The radiation flux at the sample was considerably higher than in Ref. [5]. The distribution of heating radiation on the foil sample was inhomogeneous due to close arrangement of the foil sample relative to the emitting end face of pinch with a diameter of 0.5 mm. Incident energy flux heated the foil area of 0.5 mm in diameter up to a temperature of 156 eV. The transmission was measured by comparing the spectrum of the 20-μm-thick plastic foil, containing Fe/Mg with the spectrum of a similar foil without Fe/Mg in subsequent shots. The absorption spectrum at a Fe/Mg density of 7×10^{21} cm^{-3} was measured in the photon energy range of 800–1800 eV.

In Ref. [7], we have measured the transmittance of Al plasmas, heated by Z-pinch radiation by using a facility less powerful than in Refs. [5,6]. Al plasma was produced by heating a 0.75-μm Al foil. Three spectra were recorded simultaneously in each shot: (a) a spectrum of the Z-pinch, (b) a spectrum of the Z-pinch passed through hot Al plasma, and (c) a spectrum of the Z-pinch, passed through the cold Al foil placed at a large distance from Z-pinch. The foil, producing Al plasma, was placed parallel to the discharge axis at a distance of 11 mm from it and perpendicular to the radiation flux. A typical pinch diameter of 1–1.5 mm was considerably smaller than the distance to the foil. Advantages of such geometry were absence of plasma and electron beam fluxes at the sample position, and that the geometry provided quite homogeneous irradiation of foils compared to Ref. [6]. One more advantage of this geometry was that a relatively small distance from the radiation source provided foils heating up to 30 eV that led to an enormous increasing of the transmission in the range of 6–17 nm. There was a strong magnetic field of ~200 T parallel to the foil surface at this position. It required that the Al plasma expansion in the direction perpendicular to the foil was measured. Interpretation of the absorption line spectra allowed one to obtain important information about parameters of Al plasmas. Radiation-gas-dynamics simulations performed in Ref. [7] were in accordance with these data and gave the spectral transmission of Al plasmas that was in good agreement with the experimental data.

The present work is a continuation of Ref. [7]. Its main purpose is to present new and considerably more detailed information about obtained experimental results, interpretation of spectral data and radiation-gas-dynamics simulations.

2. Experiment setup

To produce a high-power Z-pinch, we use the Angara-5-1 facility with a current of up to 4 MA [10]. The experimental setup is shown in Fig. 1. High-power EUV radiation formed by implosion of W wire arrays is used both for heating thin Al foils and probing Al plasma layer. The foil thickness is

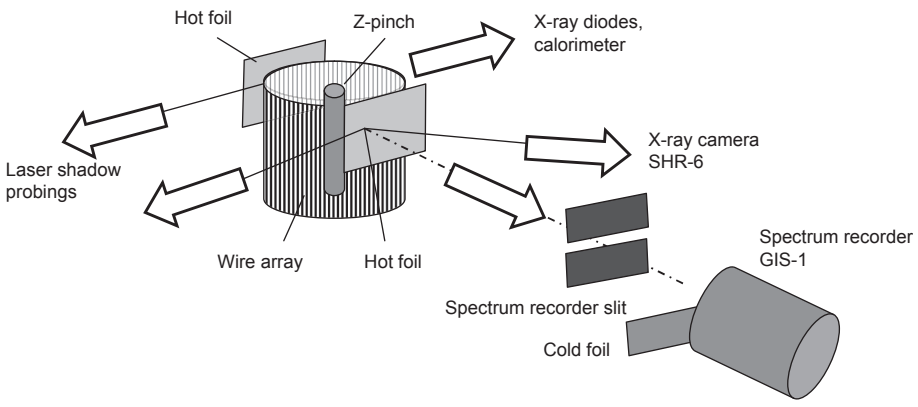

Fig. 1. Schematic diagram of experiments on studying the radiation heating of Al foils.

0.75 μm (an area density of 202.5 μg/cm^2). Two types of similar Al foils are used in experiments: a so-called "hot" foil, which is set at a distance of $R = 11$ mm from the pinch axis, and a "cold" foil, which is set at a significantly large distance from the radiation source, ranging from dozens of centimeters to two meters. The latter foil is served as a control channel recording the Z-pinch radiation passes through a conventional solid-state Al filter, whereas the former one is used to produce Al plasmas. Peak intensities of heating radiation on "hot" foil surfaces in these experiments are in the range of 0.19–0.54 TW/cm^2 with a maximum total flux of ~6 kJ/cm^2. Fig. 2 presents the layout of "hot" Al foil samples, tungsten wire array and SHR-6 camera, where the "cold" foil is not shown, because it is far away from the part of the experimental setup shown.

Radiation of the Z-pinch is analyzed by means of three vacuum X-ray photodiodes with a time-resolution of 1 ns [11] equipped with X-ray filters. The total energy of Z-pinch radiation is measured by a calorimeter [12]. A spatial structure of the radiation that passes through hot and cold foils, and the radiation of the hot foil itself are investigated by using three time-integrated X-ray pinhole cameras with a filter of 2-μm mylar, a filter of 0.75-μm Al, and without filters respectively.

Two-dimensional images are recorded by the SHR-6 recorder (6 frames, frame exposition time of ~2 ns, $\lambda < 60$ nm). The spectral characteristic of the SHR-6 camera is presented in Fig. 3. Thus, the SHR-6 camera records images of plasmas in the most energy-intensive spectral range of radiation on the Angara-5-1 facility (marked by the gray rectangle in Fig. 3). The spatial resolution on an object (foil) is 100–200 μm for photons in the wavelengths range of 4–12 nm. Dynamics of plasma expansion of the hot foil is investigated by means of multi-frame X-ray photography using the SHR-6 camera and by 3-frame 532-nm laser shadow photography with a frame exposure time of 0.6 ns.

Two similar "hot" foils are placed at the same distance of 11 mm from the axis of the pinch oppositely to each other (see Figs. 1 and 2). The foils are slightly bent for laser shadowgraph observation of only the middle part of the face and the rear surface in order to exclude the influence of edge effects on image recording. The chosen observation directions (along the front surface of one bent foil and along the rear surface of the other foil) allow one to measure displacements of foil plasma edges in the direction normal to the front and rear surfaces of two foils in each shot, excluding edge effects.

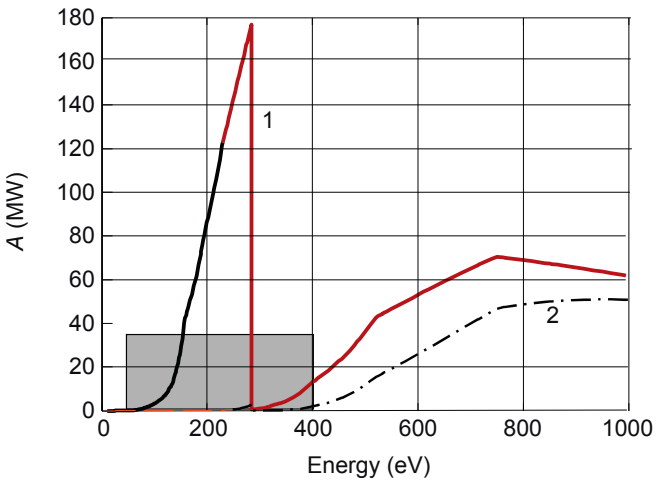

Fig. 3. Spectral sensitivities of X-ray pinhole camera SHR-6: 1 – spectral sensitivity of SHR-6 with 1-μm-thick polypropylene filter; 2 – spectral sensitivity of SHR-6 with 1-μm-thick polypropylene filter along with 0.75-μm-thick Al foil. The gray rectangle shows the most representative spectral energy range for tungsten wire array radiation of Angara-5-1 facility.

Simultaneous EUV-spectra of Z-pinch radiation and spectra of the radiation passed through hot and cold foils are recorded by an off-Rowland grazing incidence spectrograph GIS-1 [13,14,16]. In the GIS-1 scheme, spectra are recorded in a plane normal to diffracting rays (see Fig. 4). Exact focusing is only possible at one wavelength λ_0 corresponding to the point of intersection between the registration plane and the Rowland circle. However, due to a small numerical aperture of the spectrograph, it is possible to record the spectrum in a sufficiently wide spectral range $\lambda_0 \pm \Delta\lambda$. The parameter $\Delta\lambda$ is related with the observed spectral resolution $\lambda/\delta\lambda$: the wider

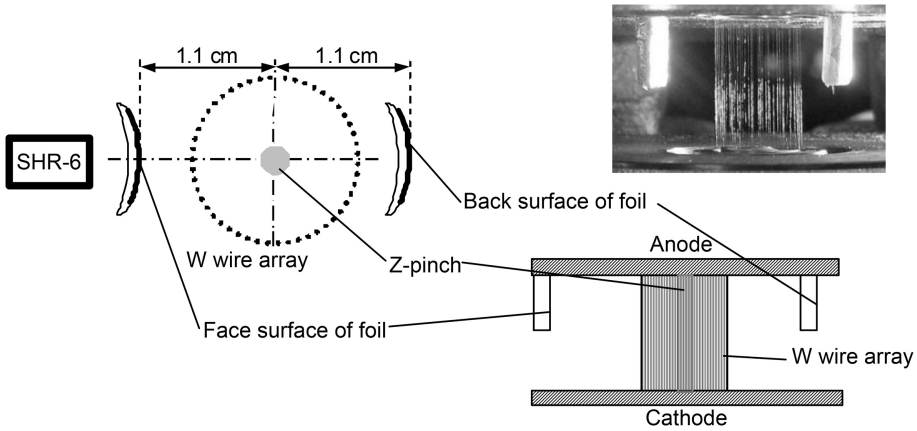

Fig. 2. Layout of the Al foil samples, tungsten array and SHR-6 camera for observation through the "hot" foil. The pinholes of SHR-6 are located at a distance of 1.623 m from the pinch center.

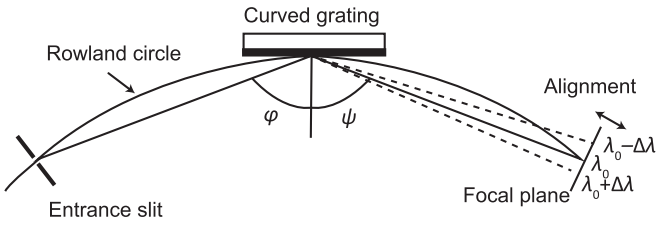

Fig. 4. Scheme of grazing incidence spectrograph (GIS-1). φ − incidence angle, ψ − diffraction angle, λ_0 − central wavelength.

$\Delta\lambda$, the lower $\lambda/\delta\lambda$ caused by defocusing. Alignment at a different λ_0 is realized by changing the distance between the plane of registration and grating. The device used has such advantages as structural simplicity, unnecessary adjustment of elements on the Rowland's circle and high luminosity at the central wavelength λ_0.

The spectrograph comprises a metal housing and a removable plug-in unit with a detector. An entrance slit and a 600-grooves/mm diffraction grating (with the radius $R = 1$ m, grazing angle of 4°, W/Re coating) are installed in the housing. An additional diaphragm installed between the entrance slit and grating is used for reducing the angular aperture. A UF-4 photographic film is chosen as the detector because it is not sensitive to the electromagnetic interference. Due to very small dimensions, the spectrograph is installed in a standard $\phi = 60$ mm optical mount.

Preliminarily the film is calibrated in a spectral range of 5−20 nm by using a vacuum ultraviolet (VUV) reflectometer based on capillary discharge plasmas [14]. Calibrated data are given in Ref. [15]. The film density is transformed in the intensity scale by using the UF-4 characteristic curve [15]. Preliminary calibration of the diffraction grating shows that the second- and third-order reflections at wavelengths $\lambda = 8$−10 nm do not exceed 10% of the first-order reflection intensity.

The spectrograph is placed at a distance $x \sim 1.54$ m from the discharge axis. An additional spatial slit is placed in front of the spectrograph. This slit makes it possible to record simultaneously on the same photographic film the time-integrated EUV spectra of Z-pinch radiation along with the spectra of radiation passed through the "hot" and "cold" foils. EUV spectra are investigated in the wavelength range $\lambda = 2$−30 nm with the maximal resolution of $\lambda/\delta\lambda \sim 100$. The wavelength scale of spectra was reconstructed using a dispersion curve for GIS-1 spectrograph.

To use the spectrograph most efficiently, a reliable alignment procedure for the vacuum chamber is developed. The instrument is also protected against radiation, shock waves and explosion products from the main discharge. In particular, to shield the instrument from X-ray radiation, special screens with a lead thickness of 3 cm are used.

3. Experimental results

The radiating pinch has a diameter of ~1.5 mm and length of 16 mm. The size of the emitting part of the pinch is recorded by pinhole cameras and the SHR-6 recorder.

Previous analysis shows that pinch emission consists of two components. The first softer and longer component has a full-width half-maximum (FWHM) duration of about 20−30 ns. This emission starts 5−10 ns prior to the beginning of a harder-radiation peak. The spectrum of the second component with a FWHM duration of 5−7 ns is harder. The two components overlap and have comparable full energies.

Time-integrated images of the pinch observed through a "hot" foil and then through various filters are shown in Fig. 5. Those are obtained with three pinhole cameras in a single shot. Each frame (a), (b) or (c) corresponds to a specific pinhole camera. The pinhole cameras differ by the filters covering the pinholes. Frame (a) corresponds to the pinhole without filters; frame (b) corresponds to the pinhole with a 2-μm mylar filter and the spectral range $\lambda < 10$ nm, and frame (c) corresponds to the pinhole with a 0.75-μm Al filter and the spectral range $\lambda > 18$ nm. Fig. 5(d) shows filter transmissions versus photon energy in the unit of eV, where curve 1 corresponds to the pinhole image in frame (b) with the 2-μm mylar filter, whereas curve 2 corresponds to frame (c) with the 0.75-μm Al filter.

Spatial-temporal structure of the intensity of pinch emission passed through the "hot" and "cold" foils, is presented in Fig. 6. A linear mass of the array comprised of 40 tungsten wires is 330 μg/cm in this shot. The array diameter and height are 10 cm and 16 mm, respectively. Time dependence of the output EUV radiation pulsed power received in the energy range of photons with $h\nu > 100$ eV in shot No. 5576 is presented in Fig. 6(b).

Fig. 6(a) shows 6 frames obtained by the pinhole camera SHR-6 with an exposure time of 2 ns. Time marks on the X-ray pulse corresponding to the frames are shown in Fig. 6(b)

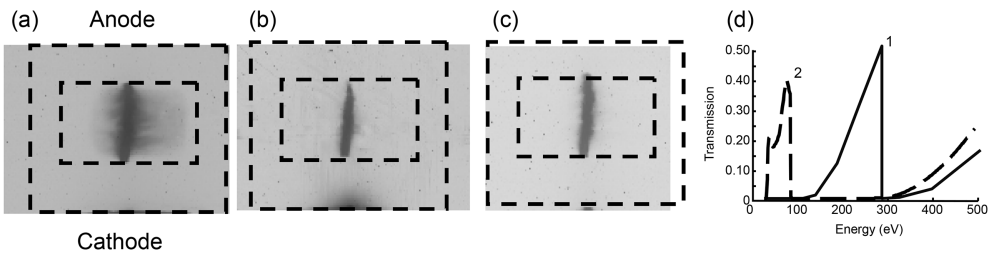

Fig. 5. Images of the Z-pinch obtained on X-ray films by three filtered pinhole cameras with a plastic frame with a 0.75 μm Al-foil. Negative images. Shot 5569. (a) without a filter; (b) with the 2-μm mylar filter; (c) with the 0.75-μm Al filter; (d) spectral transmission of filters: 1 − 2-μm-thick mylar film, 2 − 0.75-μm-thick Al foil.

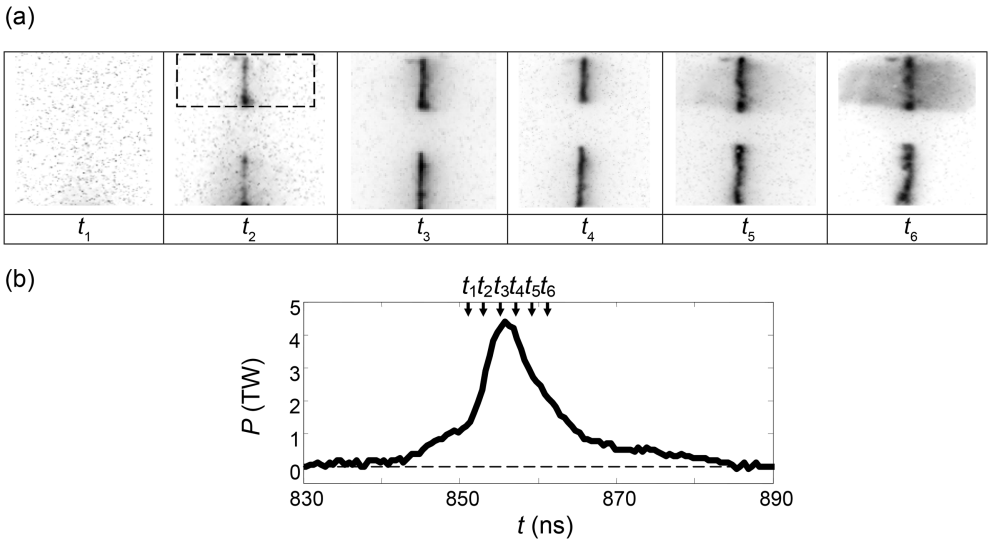

Fig. 6. (a) SHR-6 images of pinch emission passed through the "hot" Al foil (upper part of each frame) and "cold" foil (bottom part of each frame). The gap between the upper and lower images is related to a plastic frame onto which the aluminum foil is glued. Dotted rectangle marks edges of "hot" foil. (b) Time dependence of pinch radiation power. Arrows indicate the timing of SHR-6 frames.

by arrows. The upper part of pinch images in each frame is covered by the "hot" foil, whereas the bottom part is covered by the "cold" foil with the same thickness located at a distance of 15 cm from the pinch. The X-ray camera SHR-6 has a gold photocathode and a 1-μm-thick protective polypropylene film. This camera has two sensitivity ranges of 4–12 nm and 0.1–3 nm in the spectrum range of interest. Only the radiation of the second range passes through the cold foil. As one can see from Fig. 6(a), the image of the central hottest pinch part appears in the second frame and colder peripheral plasma in the upper pinch part is observed from the fifth to sixth frames. This behavior is explained by the fact that the transmission of hot plasmas increases starting from the fifth or sixth frame, and the range of 4–12 nm also contributes to the image. Observation of the image of peripheral plasma through the foil indicates that the intensity of foil intrinsic radiation in the sensitivity range of SHR-6 is low.

The dynamics of expansion of the face (to the pinch) and rear surfaces of the "hot" foil at different instants are also studied by using the laser shadow probing along the rays parallel to foil surfaces. Our estimates show that, as observed in shadow images, the sharp edge of the "shadow" of Al plasmas has been formed by effects of refraction and absorption in undercritical plasmas, leading to laser ray escaping from the aperture, and not by its reflection on its critical surface. Several measured positions of image borders allow one to estimate border expansion velocities, which are 90–100 km/s on the face surface and 40–60 km/s on the rear one.

We have studied the time-integrated spectra of Z-pinch plasma radiation and of the same radiation passed through the hot and cold foils. The hot foil heated by the pinch radiation has the size of 6 mm × 8 mm and is placed at a distance of $R = 11$ mm from the Z-pinch axis. The cold foil is placed inside the spectrograph directly in front of a photographic film.

A spectrum of Z-pinch plasma is presented in Fig. 7. The spectrum is observed in the (-1) diffraction order (for diffraction angles $|\psi| < |\varphi|$, φ is the angle of incidence) and in the $(+1)$ order (for diffraction angles $|\psi| > |\varphi|$). In the (-1) order, the intensity maximum is observed at a wavelength $\lambda_{max} \sim (6–7)$ nm with a smooth intensity decrease at long wavelengths and sharp fall at short wavelengths. The last effect at wavelengths $\lambda < \lambda_{max}$ is explained by sharp reduction of grating efficiency in a short-wavelength range rather than by intensity distribution of Z-pinch plasmas itself. This is confirmed by the intensity distribution in the spectrum recorded in the $(+1)$-order (see Fig. 7). This order is characterized by the cut-off wavelength $\lambda_c \sim 3$ nm corresponding to the diffraction angle $\psi = 90°$. The large diffraction angle (or small

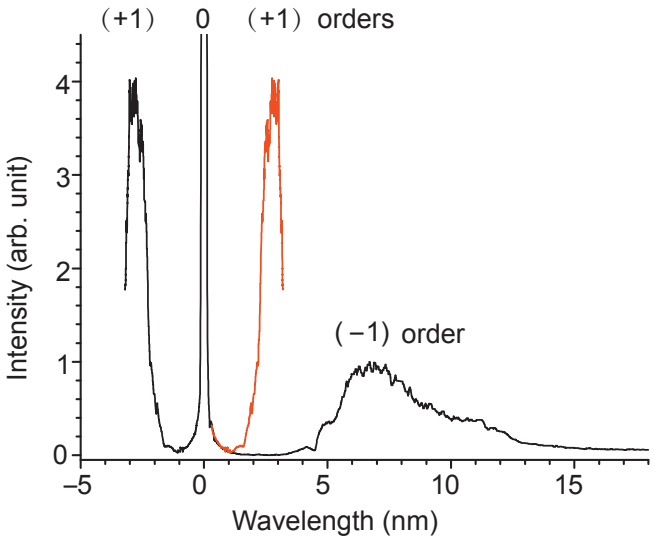

Fig. 7. The spectrum of Z-pinch plasmas recorded in $(+1)$ and (-1) − diffraction orders. The red spectrum is $(+1)$-order inverted relative to the zero-order.

grazing diffraction angle $\psi^* = 90^\circ - \psi$) leads to a higher reflection coefficient of the diffraction grating. Thus high intensity level in the wavelength range of $\lambda \sim 2$–3 nm is observed in the (+1)-order, while it is not the case in the (−1)-order. The intensity maximum in the (+1)-order corresponds to the wavelength $\lambda_{max} \sim 3$ nm.

As a result, one may conclude that the maximum of intensity distribution of Z-pinch plasma radiation is located at least in a wavelength range ranging from $\lambda \sim 3$ nm ((+1)-order data) to $\lambda \sim 7$ nm ((−1)-order data). This conclusion is important for validating theoretical fittings to experimental spectra.

Spectral analysis of radiation passed through the cold foil shows that the foil starts to transmit radiation from a wavelength $\lambda > 17$ nm. This wavelength corresponds to the L-absorption edge of neutral Al. No radiation passing through the cold foil has been detected in a shorter wavelength range ($\lambda \sim 5$–17 nm). This observation qualitatively corresponds to the calculated transmittance: ~12%–32% of the 0.75-μm-thick cold foil in the long-wavelength range of L edge and $<10^{-8}$ at wavelengths $\lambda \sim 8$ nm [17].

Fig. 8 shows a Z-pinch source spectrum passed though the "hot" foil. Comparing spectral transmissions of filters in Fig. 5(d) and the spectrum in Fig. 8, one may conclude that the image in Fig. 5(a) may be formed by radiation pertaining to the whole spectral range of 5–25 nm. Fig. 5(c) (behind the "cold" Al filter) is formed by radiation pertaining to the spectral range of 5–8.6 nm, whereas Fig. 5(b) (behind the mylar filter) is formed by radiation pertaining to the spectral range of 16–25 nm. One can see that Fig. 5(a) comprises a central part of the pinch and a halo surrounding it. Due to time integration, the halo is substantially formed by the main part of pinch plasmas prior to the instant of maximum compression. Contribution of peripheral plasmas to the image in Fig. 5(a) may be negligible. The radial size of Fig. 5(a) is considerably less than the transverse size of the "hot" foil. As a result, one may conclude that the intrinsic radiation of the "hot" foil may give minor contribution to the spectral range of 5–12 nm. The intrinsic radiation of the "hot" foil will be seen in Fig. 5(a) as a uniform rectangle inside the plastic holder that is shown in Fig. 5(a)–(c) as dashed rectangles. One may also conclude that the halo is formed mainly by the radiation pertaining to the spectral range of 8.6–15 nm (or 80–150 eV).

Spectra of radiation passed through the hot foil are quite different: radiation in a shorter wavelength range from the L-edge of neutral Al with wavelengths of $\lambda \sim 6$–17 nm has been observed (see Fig. 8). Experimental transmission of the "hot" foil versus radiation wavelength is shown in Fig. 9. Transmission is obtained as a ratio of the spectrum in Fig. 8 and the direct spectrum of the Z-pinch obtained in the same shot. Fig. 9 shows just the same value, however, calculated using the results of plasma dynamic simulation obtained in Section 5. Induced transparency in the wavelength range of 6–17 nm is clearly observed in Fig. 9. This is one of the main qualitative results of the present work.

Absorption lines are also clearly observed in the experimental transmission spectrum in Fig. 9. Observed absorption lines indicate that this spectrum is indeed a spectrum of tungsten Z-pinch radiation passed through the "hot" foil rather than the spectrum of intrinsic radiation of the hot foil. The similar conclusion has been made above while analyzing images from the pinhole cameras.

Note that the intensity of radiation passed through the hot foil, and a spectrum of radiation incident to the foil are linear functions of the reflection coefficient for the diffraction grating. The ratio of these intensities, which is the foil transmittance, is independent of the grating reflection coefficient.

The lowest experimental error (±25%) of determining transmission of the hot foil is observed in the spectral range of $\lambda \sim 8$–13 nm. This range corresponds to the maximal detected intensity of radiation passed through the foil (Fig. 8). The experimental transmission in the long-wavelength range of $\lambda \geq 13$ nm is probably underestimated. This can be explained by two reasons. The first is a low detected intensity of the radiation passed through the foil. The second is a high-diffraction-order contribution to the intensity of radiation incident to the foil with respect to which the intensity of passed radiation is normalized.

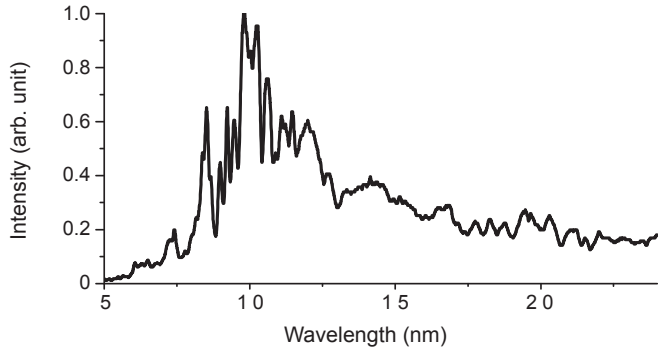

Fig. 8. Typical experimental spectrum of Z-pinch back illuminator transmitted through the "hot" Al-foil.

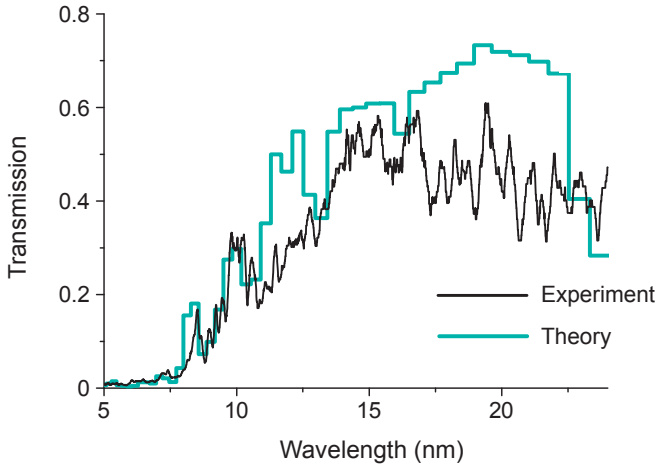

Fig. 9. Experimental and simulated transmission of the "hot" Al-foil versus wavelength.

4. Modeling of absorption spectra

To describe the structure of spectrum of Z-pinch plasma radiation passed through the hot foil, additional calculations have been performed. These calculations include the study of ion charge distribution, determination of the wavelengths and oscillator strengths for transitions in Al ions, and Al spectrum modeling at various electron temperatures T_e, densities N_e with different spectral resolutions. The codes FLEXIBLE ATOMIC CODE [18], FLYCHK [19] and INDAHAUS are used for this purpose. Calculations for $N_e = 2 \times 10^{20}$ cm^{-3} and $T_e = (15–30)$ eV show that Al ions with charges from 4+ to 7+ contribute to the absorption spectrum. The best accordance between the structures of experimental and theoretical spectra in the spectrum range of $\lambda = (5–14)$ nm is observed for the calculated spectrum at $T_e = 22$ eV (see Fig. 10). The absorption lines are identified as transitions 3–2, 4–2, 5–2 in ions Al^{4+}, Al^{5+}, Al^{6+}, Al^{7+} with relative ion concentrations of 10%, 45%, 41% and 4%, respectively. Thus, Al foil heating by radiation leads to the formation of plasmas with a temperature $T_e \sim 20$ eV, and the most represented ions are Al^{5+} and Al^{6+}. Such foil transmission substantially rises in the short wavelength range of L-edge absorption. In the case of "hot" foil, the effect of induced transparency is observed experimentally when the transmittance at the short wavelength range of absorption L-edge increases from 10^{-8} for the cold foil to 0.2–0.3.

5. Simulation of expansion of foil heated by radiation

Heating and expansion of the Al foil irradiated by high-intensity radiation from the Z-pinch are simulated by using the two-dimensional radiation gas-dynamic code RALEF2D [8,9]. This code solves equations of hydrodynamics with heat conduction and thermal radiation spectral transfer. The intensity of radiation at each space-time point is considered as a function of directions in 3D physical space and of photon energy. Matter radiation-induced heating and cooling are self-consistent in the code with the spectral, angular, and spatial radiation transport. Radiation transport is treated within the steady-state transport equation in each moment with the Planckian source function and the spectral mean free paths of radiation, which are specified in tables preliminarily obtained using the THERMOS code [20]. This code implements the quantum statistical model of the hot matter described in Ref. [20] and provides not only optical but also thermodynamic parameters for the RALEF2D code. The RALEF2D code is used for simulating radiation properties of pinch and laser plasmas (see, e.g. [16,21–23]).

In the simulation, the cold Al foil with an initial thickness of 0.75 μm is irradiated by a radiation flux normally incident onto its surface. The initiating radiation consists of two components with different spectra and time profiles. The first component that is colder and longer than the second one, and is smoothly decreasing with time, has the spectrum corresponding to the Planckian spectrum with a temperature of 45 eV. The power profile on the irradiated side is specified by the formula:

$$P_1(t_{ns}) = \frac{7\, t_{ns}}{1 + (t_{ns}/12.5)^3} \ \left[\mathrm{MW/cm^2}\right] \quad (1)$$

The subscript "ns" means that time t in this equation is measured in nanoseconds. The second component of the radiation pulse that is faster and harder than the first one has the spectrum corresponding to the Planckian spectrum with a temperature of 70 eV, whereas the time profile of the power is specified by the expression:

$$P_2(t_{ns}) = 0.38\, t_{ns} \exp\left(-\frac{t_{ns}}{1.88}\right) \ \left[\mathrm{TW/cm^2}\right] \quad (2)$$

The second harder pulse is delayed by 7 ns with respect to the softer pulse. The total energy in the pulse is 2.3 kJ/cm^2 and

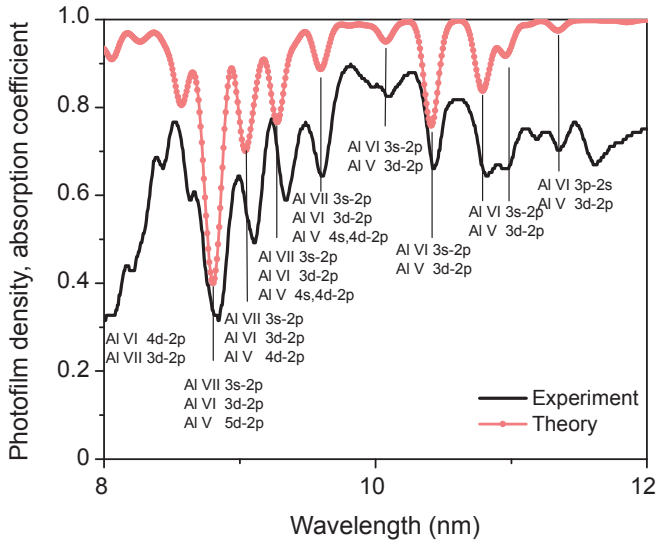

Fig. 10. Comparison of the spectrum of Z-pinch radiation passed through the "hot" foil (in units of photographic density on photofilm) (black) with calculated spectrum (the absorption coefficient in relative units, normalized to the strongest transition 2p–3d in Al^{5+} ion) at temperature $T_e = 22$ eV (red).

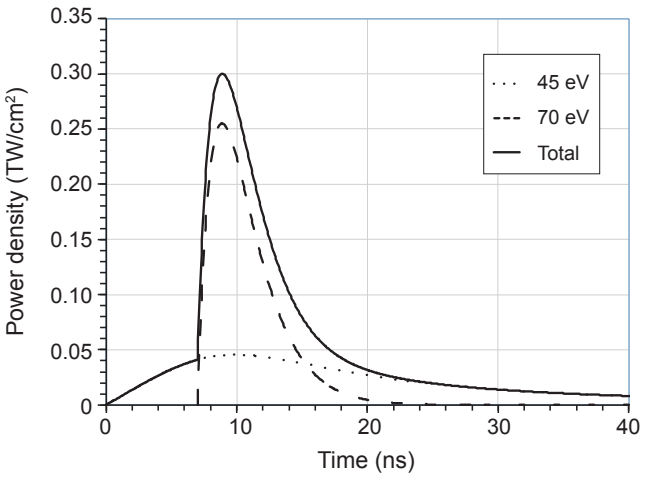

Fig. 11. Temporal profile used for calculating the power of radiation falling on the foil.

is almost equally distributed between both pulse components. The peak power density incident onto the foil is 0.3 TW/cm^2. The resulting power density profile of the radiation incident on the foil used in the simulation is shown in Fig. 11. A time-integrated spectrum of the radiation is shown in Fig. 12. We have also made a second version of simulation. It differs from the first version described above by that the powers of both heating pulse components are increased in parallel so that the peak power become 0.5 TW/cm^2. Incident radiation spectra in both versions are similar. The Planckian temperatures used are approximately close to temperatures of the blackbody radiation corresponding to the power and dimensions of the source. We do not state that the real spectrum of the Z-pinch has a blackbody shape, but believe that its spectral characteristics in the simulation qualitatively correspond to those in the experiment.

Simulation with the 0.3 TW/cm^2 peak power shows that the foil under irradiation is heated, ionized, and rapidly expands. The outer layers of the foil facing the pinch are rapidly heated to temperatures of about 20–30 eV. The radiation of the pinch heats matter on the other side also. Nevertheless, heat conduction and radiation transfer in the expanding foil make a larger contribution to the heating of these plasma layers. Plasmas on the rear side of the foil is noticeably heated (to temperatures of about 10 eV) already after reaching the peak power of the radiation heating the foil. The average charge of ions on the rear side of the foil at the time of the peak power is +3. In about 3 ns after this moment, when the power of the heating radiation decreases approximately by 40%, the average charge of ions on the rear side increases to +6.3 (at a plasma temperature of about 19 eV). These features indicate that a noticeable amount of Al ions with charges from +4 to +7 can present on the rear side of the foil immediately after the peak power. This corresponds to the above theoretical analysis of the experimentally detected absorption lines and indirectly indicates that our simulation of heating and expansion of the foil is adequate. Figs. 13 and 14 show the spatial distributions of plasma parameters at the moments of $t = 9$ and 12 ns after the start of the heating pulse in the simulation.

The other results of the simulation that can be directly compared to the experiment are as follows. The simulation gives a time-integrated radiation spectrum of the pinch passed through the foil. The time-integrated spectrum of the incident radiation is known from the input parameters of the simulation. The ratio of these two spectra gives the effective integral spectral transmittance for the foil, which is shown in Fig. 9. As in the experiment, very strong induced transmittance of Al foil is observed in the wavelength range of 5–24 nm. The simulated contribution of the foil intrinsic radiation is small in this spectral range. Fig. 15 shows the comparison of the integrated transmission of Al foils in two different simulations, with 0.3 and 0.5 TW/cm^2 peak powers.

Fig. 16 shows both the simulated spectrum of the pinch radiation passed through the hot Al foil and the simulated spectrum of intrinsic radiation of the hot foil. The angular density of the intrinsic radiation per steradian is shown only

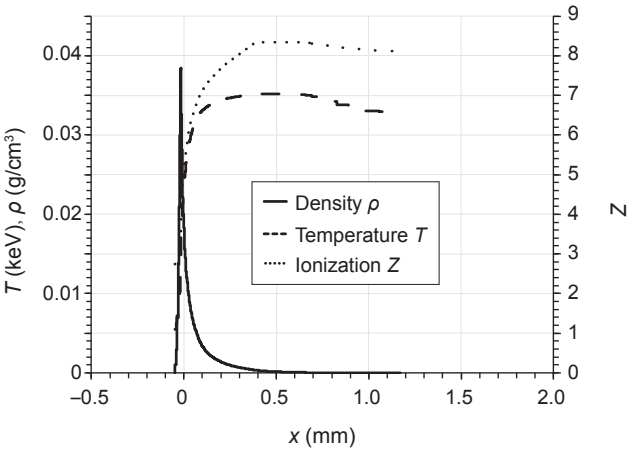

Fig. 13. Simulated distributions of plasma parameters across the plasma layer at $t = 9$ ns: density (ρ), temperature (T), and mean ionization (Z) of Al.

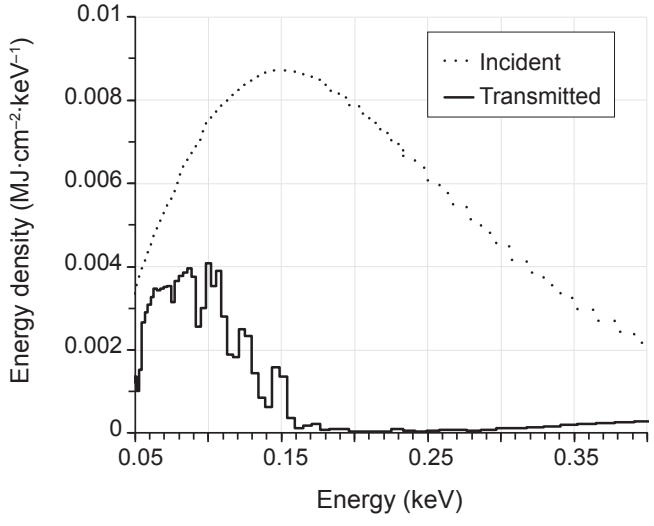

Fig. 12. Simulated time-integrated spectrum of radiation incident on the foil and simulated time-integrated spectrum of pinch radiation transmitted through the foil. The intrinsic radiation of foil plasma is extracted from the latter spectrum.

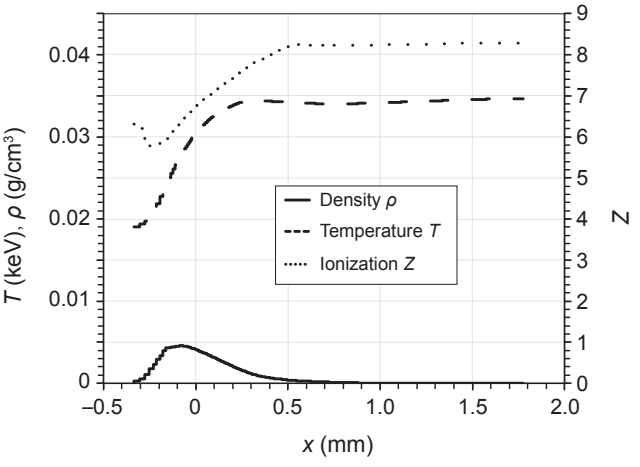

Fig. 14. Simulated distributions of plasma parameters across the plasma layer at $t = 12$ ns: density (ρ), temperature (T), and mean ionization (Z) of Al.

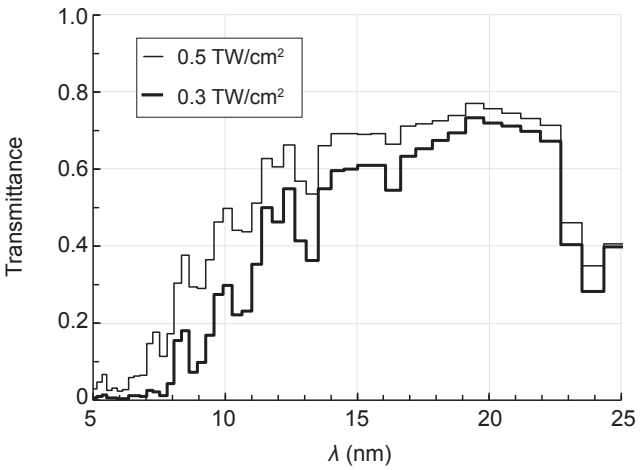

Fig. 15. Comparison of simulated time-integrated spectral transmittances versus wavelength for two different simulations with 0.3 and 0.5 TW/cm^2 peak powers of heating radiation.

for the direction perpendicular to the foil surface and parallel to the direction of the pinch radiation. The intrinsic radiation is extracted from full radiation, when we calculate the pinch spectrum passed through the hot foil. To compare them, it is necessary to keep in mind that these two components of the full radiation at the rear side of the hot foil have quite different angular distributions. For this reason, the values shown in Fig. 16 have different dimensions.

The experimental and theoretical transmittances are in good agreement (within ±25%) in the spectral range corresponding to the maximum detected intensity of the absorption spectrum ($\lambda = 8-13$ nm) (see Fig. 9). The theoretical opacity in the long wavelength range of the spectrum ($\lambda \geq 13$ nm) is larger than the experimental value by a factor of about 1.5−2.

The effective velocity of expansion of the foil can be determined from the positions, where the density of Al plasmas is half the maximum Al plasma density at each instant. We may compare this velocity with the expansion velocity derived from the laser shadow images obtained along the directions almost parallel to the surface of the foil. We expect that such an approach to theoretical expansion of the hot foil can qualitatively reflect a complicated process of "shadow" formation in the experiment. The effective average rates of foil expansion in the time interval from the peak heating radiation power to the instant 20 ns later, which are thus calculated, are ~80 km/s on the face side and ~70 km/s on the rear side. These velocities qualitatively agree with the above results of the transverse laser shadow probing of the foil.

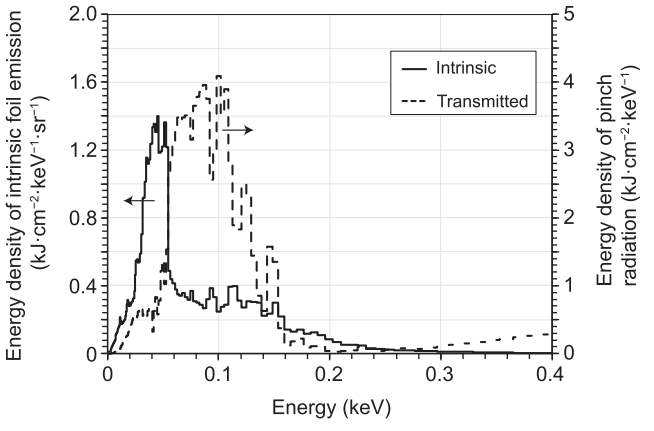

Fig. 16. Comparison of simulated spectra of intrinsic foil emission in the direction perpendicular to its surface and simulated spectra of the pinch emission passed through the foil. These radiation fluxes have quite different angular distributions. As a result, these two values have different dimensions that should be taken into account for quantitative comparison.

6. Conclusions

We have measured the absorption of EUV-radiation in the range of wavelengths 5−24 nm in Al plasmas in a new experimental geometry. This geometry has resulted in foil heating up to a temperature of 30 eV and in a density of about 1−20 mg/cm^3. This temperature is about the same as in Ref. [6], while the radiation power is several times lower. Tungsten Z-pinch of Angara-5-1 has produced uniform illumination of the foil with 0.55 TW/cm^2 without plasmas flowed from the pinch. The same radiation is used as a probing for studying dependence of transparency of hot foil versus wavelength. Several measurements have been made in the same shot:

- A spectrum of the pinch radiation;
- A spectrum of the pinch radiation that has passed through the Al plasma heated by it;
- A spectrum of the pinch radiation that has passed through the cold foil which allows one to certainly observe the effect of induced transparency of thin Al foils in the process of radiation heating by powerful EUV radiation.

It has been demonstrated that in the wavelength range of 6−17 nm, transmission in heated Al plasma increases by several orders compared to that in cold Al. The laser probing of face and rear sides of the heated foil is compared with the results of simulations. Simulations of the model spectrum of absorption in homogeneous Al plasmas allow one to interpret the recorded absorption lines. Simulations of Al foil heating and the expansion with self-coordinated spectrum transition of the foil intrinsic radiation, as well as the heating radiation, are also performed. The shapes of time integrated simulated and measured transmission spectra coincide with an accuracy of 30%. Similar shapes confirm the theoretical model [20] of the absorption coefficient in Al plasmas. The experimental results correspond well to the interpretation of the recorded absorption lines and to simulations of Al foil heating and expanding with self-consistent transfer of radiation.

We make a qualitative conclusion that the intrinsic radiation of the "hot" foil makes a small contribution to the radiation behind the "hot" foil in the spectral range of 5−25 nm. Nevertheless, quantitative investigation of this part of radiation is necessary in further works. Probably, it will not require new techniques.

Presented results show that the experimental technique can be applied to studying radiation absorption in hot dense plasmas composing of other elements as well.

Acknowledgments

The work was partially supported by RSF under Grant No. 16-12-10487 and by the RFBR project 15-02-04411 and 15-01-06195.

References

[1] J.M. Foster, D.J. Hoarty, C.C. Smith, P.A. Rosen, S.J. Davidson, et al., L-shell absorption spectrum of an open-M-shell germanium plasma: Comparison of experimental data with a detailed configuration accounting calculation, Phys. Rev. Lett. 67 (1991) 3255.

[2] T.S. Perry, S.J. Davidson, F.J.D. Serduke, D.R. Bach, C.C. Smith, et al., Opacity measurements in a hot dense medium, Phys. Rev. Lett. 67 (1991) 3784−3788.

[3] C. Chenais-Popovics, F. Gilleron, M. Fajardo, H. Merdji, T. Misalla, et al., Radiative heating of B, Al and Ni thin foils at 15−25 eV temperatures, JQSRT 65 (2000) 117−133.

[4] S.V. Bondarenko, R.V. Garanin, N.V. Zhidkov, A.V. Pinegin, N.A. Suslov, Experimental investigation of X-ray spectral absorption coefficients in heated Al and Ge on the Iskra-5 laser facility, Quantum Electron. 42 (2012) 51−57.

[5] P.T. Springer, K.L. Wong, C.A. Iglesias, J.H. Hammer, J.L. Porter, et al., Laboratory measurement of opacity for stellar envelopes, JQSRT 58 (1997) 927−935.

[6] J.E. Bailey, G.A. Rochau, C.A. Iglesias, J. Abdallah, J.J. MacFarlane, et al., Iron-plasma transmission measurements at temperatures above 150 eV, Phys. Rev. Lett. 99 (2007) 265002.

[7] E.V. Grabovski, P.V. Sasorov, A.P. Shevelko, V.V. Aleksandrov, M.M. Basko, et al., Radiative heating of thin Al foils by intense extreme ultraviolet radiation, JETP Lett. 103 (2016) 350−356.

[8] M.M. Basko, J. Maruhn, A. Tauschwitz, An efficient cell-centered diffusion scheme for quadrilateral grids, J. Comput. Phys. 228 (2009) 2175−2193.

[9] M.M. Basko, J. Maruhn, A. Tauschwitz, GSI Scientific Report 2009: Gesellschaft fur Schwerionenforschung MBH, 2010. Darmstadt, Germany, GSI Report 2010-1, 410.

[10] Z.A. Albikov, Y.P. Velikhov, A.I. Veretennikov, V.A. Glukhikh, E.V. Grabovskii, et al., Experimental complex 'ANGARA-5-1', At. Energy 68 (1990) 26−32.

[11] A.V. Branitskiy, G.M. Oleinik, Reconstruction of the parameters of a soft X-radiation spectrum from signals of vacuum X-ray diodes, Instrum. Exp. Tech. 43 (2000) 486−492.

[12] V.V. Aleksandrov, G.S. Volkov, E.V. Grabovski, A.N. Gritsuk, N.I. Lakhtyushko, et al., Anisotropy of energy losses in high-current Z-pinches produced by the implosion of cylindrical tungsten wire arrays, Plasma Phys. Rep. 40 (2014) 135−145.

[13] A.P. Shevelko, L.A. Shmaenok, S.S. Churilov, F.J. Bastiaensen, F. Bijkerk, Extreme ultraviolet spectroscopy of a laser plasma source for lithography, Phys. Scr. 57 (1998) 276−282.

[14] A.P. Shevelko, L.V. Knight, R.S. Turley, O.F. Yakushev, An intense XUV source of radiation, within the 4-45-nm-spectral range, based on capillary discharge plasmas, Proc. SPIE 4504 (2001) 143−150.

[15] E.D. Kazakov, A.P. Shevelko, New method of treatment the UV spectra of multiply charged ions for the diagnosis of high temperature plasma, Voprosi atomnoy nauki i techniki, Termojaderny Sint. 37 (2014) 71−75.

[16] A.P. Shevelko, E.D. Kazakov, I.Yu. Tolstikhina, D.E. Bliss, M.G. Mazarakis, et al., EUV spectroscopy of plasmas created in the final anode-cathode gap of the Z-machine high-current pulsed generator (SNL), Plasma Phys. Rep. 34 (2008) 944−954.

[17] A.C. Thompson, I. Lindau, D.T. Attwood, Y. Liu, E.M. Gillikson, et al., X-ray Data Booklet, third ed., LBNL, Berkeley, 2009. http://henke.lbl.gov/optical_constants/filter2.html.

[18] M.F. Gu, The flexible atomic code, Can. J. Phys. 86 (2008) 675.

[19] H.-K. Chung, M.H. Chen, W.L. Morgan, Yu. Ralshenko, R.W. Lee, Generalized population kinetics and spectral model for rapid spectroscopic analysis for all elements, High Energy Density Phys. 1 (2005) 3−7.

[20] A.F. Nikiforov, V.G. Novikov, V.B. Uvarov, Quantum-Statistical Models of Hot Dense Matter. Methods for Computation Opacity and Equation of State (Birkhauser, Basel, Switzerland 2005).

[21] M.M. Basko, P.V. Sasorov, M. Murakami, V.G. Novikov, A.S. Grushin, One-dimensional study of the radiation-dominated implosion of a cylindrical tungsten plasma column, Plasma Phys. Control. Fusion 54 (2012) 055003−055009.

[22] A. Tauschwitz, M. Basko, A. Frank, V. Novikov, A. Grushin, et al., 2D radiation-hydrodynamics modeling of laser-plasma targets for ion stopping measurements, High Energy Density Phys. 158 (2013) 9−13.

[23] A. Frank, A. Blazevic, V. Bagnoud, M.M. Basko, M. Boerner, et al., Energy loss and charge transfer of argon in a laser-generated carbon plasma, Phys. Rev. Lett. 110 (2013) 11501.